Journal of the European Ceramic Society 20 (2000) 2735–2742

www.elsevier.com/locate/jeurceramsoc

Microwave absorption materials — IV Preparation of the mixed layer structure phases, $Re_xTa_{1-x}S_2$ and $Os_xTa_{1-x}S_2$, and some electrical and magnetic properties

K. Hayashi *, D. Serikawa, N. Maeda, A. Okamoto, T. Ikeuchi

Laboratory for Solid State Chemistry, Okayama University of Science, 1-1 Ridai-cho, Okayama 700, Japan

Abstract

The binary systems ReS_2–TaS_2 and OsS_2-TaS_2 are studied. Mixed layer structure (MLS) phases are found in $Re_xTa_{1-x}S_2$ with a composition range of $0.25 \leqslant x \leqslant 0.5$, as well as in the $Os_xTa_{1-x}S_2$ with a composition range of $0.26 \leqslant x \leqslant 0.33$. The MLSs of both phases are constructed by a random and mixed stacking of the 2Hb-layers and 3R-layers. The magnetic susceptibilities of samples from both phases show a weak Pauli-paramagnetism. The paramagnetic moment and the electrical conductivity of both phases decrease as the composition x increases. The behaviour of the paramagnetic moment and the electrical conductivity of those phases offer us a good example of the number of conduction electrons and their effect. © 2000 Elsevier Science Ltd. All rights reserved.

Keywords: Electrical conductivities; Functional applications; Magnetic properties; X-ray method

1. Introduction

Low microwave absorption materials are desired for microwave communication systems. However, high microwave absorption materials are necessary for protecting human health and digital equipment from microwave hazards. The former materials have been studied since microwave communication has been in practical use. However, the latter materials have not been studied potentially thus far. Only limited materials can be used for practical microwave absorption; these include magnetite, graphite, and metal powders. However, excellent microwave absorption materials were recently prepared in several transition metal diselenides of the MLS.[1] This high microwave absorption was experimentally related to MLSs in transition metal diselenides, and its relation should be confirmed in the other compounds.

The layered transition metal dichalcogenides show various polytypes.[2] Recently, two MLSs were reported in the $Re_xTa_{1-x}Se_2$ and $Os_xTa_{1-x}Se_2$ systems.[3] The MLSs of these system are constructed by a random and mixed stacking of 2Hb-layers and 3R-layers. As the composition x increases, two occurrences take place. First, the mixing ratio of the 2Hb-layers and 3R-layers increase, and second, the randomness of the stacking decreases. Finally, the $Re_{0.5}Ta_{0.5}Se_2$ and $Os_{0.33}Ta_{0.67}Se_2$ crystallize into the 2Hb–WSe_2 structure without any random stacking. The homogeneity ranges of the MLS phases of $Re_xTa_{1-x}Se_2$ and $Os_xTa_{1-x}Se_2$ are $0.12 \leqslant x \leqslant 0.5$ and $0.10 \leqslant x \leqslant 0.33$, respectively. The above-mentioned MLS phases show an excellent microwave absorption property.[1] The mechanism of microwave absorption for the MLS has never been explained thus far. However, we believe microwave absorption for these MLS phases may be controlled by an unknown mechanism. We must prepare new MLS compounds in order to develop microwave absorbers that diminish the electromagnetic wave hazard and establish the fundamentals of the layer stacking mechanism for the layered compounds. The MLS is essentially stabilized due to the subtle balance between two kinds of layers. Therefore, such systems are considered to be rare. The MLSs discussed in the present investigation are not structures of the meta-stable phase but structures of the stable phase.[3] There are two important chemical approaches used to investigate the layer stacking mechanism. One approach is concerned with the relationship between impurities or defects and layer stacking. The other approach is concerned with solid solutions and layer stacking. The present investigation follows the latter approach.

* Corresponding author.

PII: S0955-2219(00)00231-4

Electromagnetic wave hazard has become a serious problem because of the effect it has on computer processors and human health. There are two methods used to protect computer processors, and humans, from electromagnetic wave. One method is concerned with the reflection of the electromagnetic waves, while the other is concerned with the absorption of such. The latter method is an essential solution to the electromagnetic wave hazard. Ferrite and other graphite powders are most commonly used to absorb electromagnetic waves. Concerning electromagnetic waves of the near-microwave region, graphite powder is better than the ferrite powder. However, a 5 mm thick wall is necessary to absorb an electromagnetic wave when using graphite powder.[4] This thickness is too large and cannot be used to coat home-electronic appliances. The coating thickness can be diminished if a better absorber is prepared.

In the present investigation, two new MLS phases are prepared. The structures will be shown and the electrical conductivity and magnetic susceptibility will be reported.

2. Experimental details

2.1. Preparation

The starting materials, Ta powder (99.9% pure; Aldrich Co.), Re powder (99.9% pure; Mitsuwa Co.), Os powder (99.9% pure; Mitsuwa Co.), and S blocks (99.9999% pure; Wako Co.) were sealed in an evacuated quartz glass ampoule. The ampoule was heated at 950°C for 2 days to complete the reaction and was annealed at the desired temperatures between 600 and 1000°C for 1 week. Then a sample was obtained after quenching the ampoule in water.

2.2. Chemical composition analysis

The chemical compositions of the samples were analyzed with an electron probe microanalyser (EPMA) using the ZAF method. The Ta, M line; the Re, M line; the Os, M line; and the S, K line were used for the composition analysis.

2.3. Magnetic measurement

The magnetic susceptibility of the powder sample was measured from 5 to 300 K by the SQUID method. The applied magnetic field was 10 000 G.

2.4. Electrical resistivity measurement

The electrical resistivity was measured from 30 to 300 K on pressed powder samples using the van der Pauw method.

2.5. Powder X-ray diffraction measurement

A sample powder was processed with acetate glue to avoid the preferred orientation. After drying and grinding, the sample was mounted on the sample holder and the X-ray diffraction on the processed powder was measured.[5] Data were taken for 2 s at each 2 θ step of 0.05° from 10 to 80°.

2.6. Structure determination

Layer stacking was estimated by the simulation method. The powder X-ray diffraction pattern was simulated by using the computer programs RIETAN and SEKITAN according to the 300-layers stacking model. The random layer stacking of the structure model was made by using the Monte Carlo method. Therefore, one trial structure model was different from the other trial structure model, and the simulation pattern should be different according to the structure model. However, the reproducibility of the simulation pattern was remarkably good when the number of stacking layers exceeded 300.

3. Results and discussion

3.1. ReS_2–TaS_2 system

3.1.1. Phase diagram and structures

The phase diagram from 600 to 1000°C of the ReS_2-TaS_2 system is shown in Fig. 1. The MLS phase spreads over the composition range from $Re_{0.25}Ta_{0.75}S_2$ to $Re_{0.5}Ta_{0.5}S_2$ and the ReS_2 phase from $Re_{0.9}Ta_{0.1}S_2$ to ReS_2. Powder X-ray diffraction patterns and simulation patterns of the MLS phase are shown in Fig. 2. The sharp peaks of 00l and hk0 reflections and the broad peaks of hkl reflections are typical features of the MLS's powder X-ray diffraction pattern. The schematical

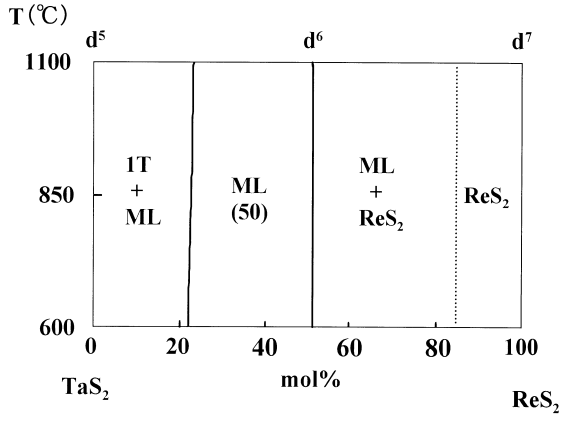

Fig. 1. Phase diagram of the TaS_2–ReS_2 system. ML: MLS phase, (50): 50% 2Hb-layers and 50% 3R-layers, 1 T: CdI_2 type structure.

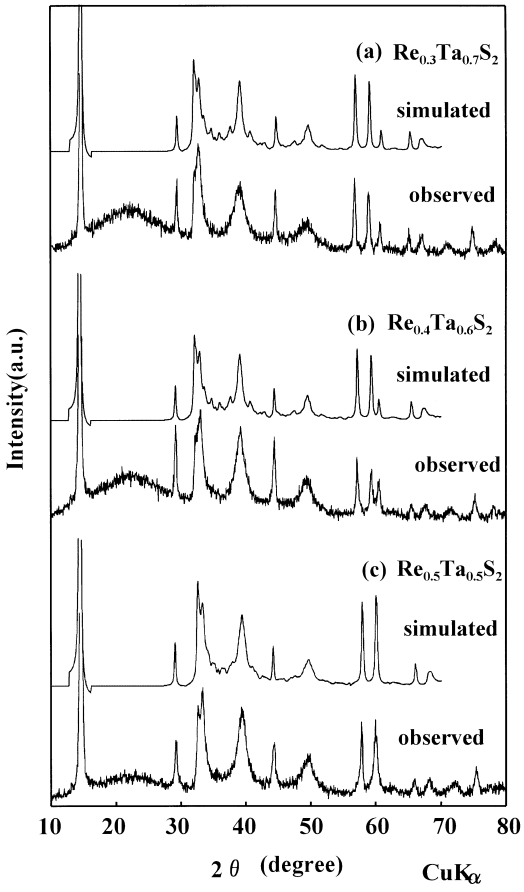

Fig. 2. X-ray powder diffraction patterns of the $Re_xTa_{1-x}S_2$ MLS phase. (a) $x=0.3$, (b) $x=0.4$, (c) $x=0.5$. Upper patterns are simulated and lower ones are observed.

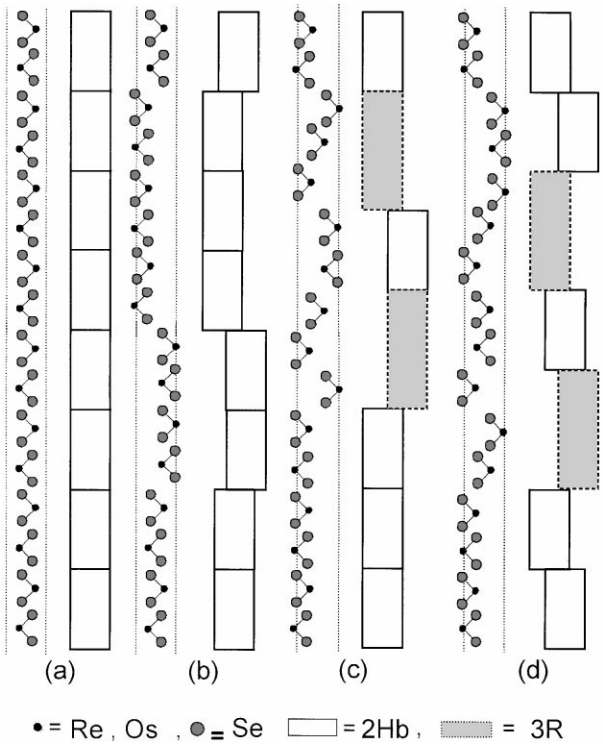

Fig. 3. Structure patterns of the MLS MX_2 compounds. (a) 2Hb–WSe_2 structure with perfect stacking of 2Hb layers, (b) 2Hb–WSe_2 structure with stacking faults, (c) MLS of 2Hb layers and 3R layers without stacking faults, (d) MLS 2Hb layers and 3R layers with stacking faults.

diagram of the MLSs and stacking fault structures is shown in Fig. 3. Pattern (a) corresponds to the perfect stacking model of WSe_2 structure; Pattern (b) the stacking fault of WSe_2; Pattern (c) the MLS of 2Hb layers and 3R layers without stacking faults between the layers; and Pattern (d) the MLS of 2Hb layers and 3R layers with stacking faults. The structure of the $Re_xTa_{1-x}S_2$ corresponds to structure pattern (d). All the simulation patterns are calculated based on the model that is used for the random stacking of 50% 2Hb-layers and 50% the 3R-layers. The fitting of the simulation patterns to the observation is satisfactory. Therefore, the MLS of $Re_xTa_{1-x}S_2$ is constructed by randomly stacking the 50% 2Hb-layers and 50% 3R-layers over the homogeneity range.

The homogeneity range of the MLS phase of $Re_xTa_{1-x}S_2$ is narrower than that of $Re_xTa_{1-x}Se_2$, because $Re_xTa_{1-x}Se_2$ is $0.12 \leqslant x \leqslant 0.5$.[3] The variants of the MLS of $Re_xTa_{1-x}S_2$ are less than those of $Re_xTa_{1-x}Se_2$, because the chemical composition and the temperature change the mixing ratio of the 2Hb-layers and 3R-layers on $Re_xTa_{1-x}Se_2$. Especially, the perfect stacking 2Hb-structure is observed on $Re_{0.5}Ta_{0.5}Se_2$ at a high temperature. At a low temperature, the composition dependence of the mixing ratio of the 2Hb-layers and 3R-layers on the $Re_xTa_{1-x}Se_2$ MLS phase is very small. Therefore, the phase relation of the sulfide system may correspond to the low temperature part of the selenide system. Generally, a sulfide system is harder than a selenide system.

The lattice parameters of the $Re_xTa_{1-x}S_2$ MLS phase are shown in Fig. 4. The c-parameter represented in the figure is reduced to that of 2Hb-polytype. The a-parameter decreases and the c-parameter and the axial ratio c/2a increase as the x-value increases. Those features of the $Re_xTa_{1-x}S_2$ MLS phase are similar to that of the $Re_xTa_{1-x}Se_2$ MLS phase. The above behaviour is common in the sulfide system and selenide system. Moreso, the elongation of the c-axis may be explained by the repulsion of the electrons of the d_z^2 orbital on a transition-metal atom against the electrons of the p_z-orbital on a sulfur atom.

3.1.2. Electrical resistivity and magnetic susceptibility

The temperature dependence of the electrical resistivity of the $Re_xTa_{1-x}S_2$ MLS phase is shown in Fig. 5. The resistivity increases as the temperature decreases. This tendency seems to be that of a semiconductor.

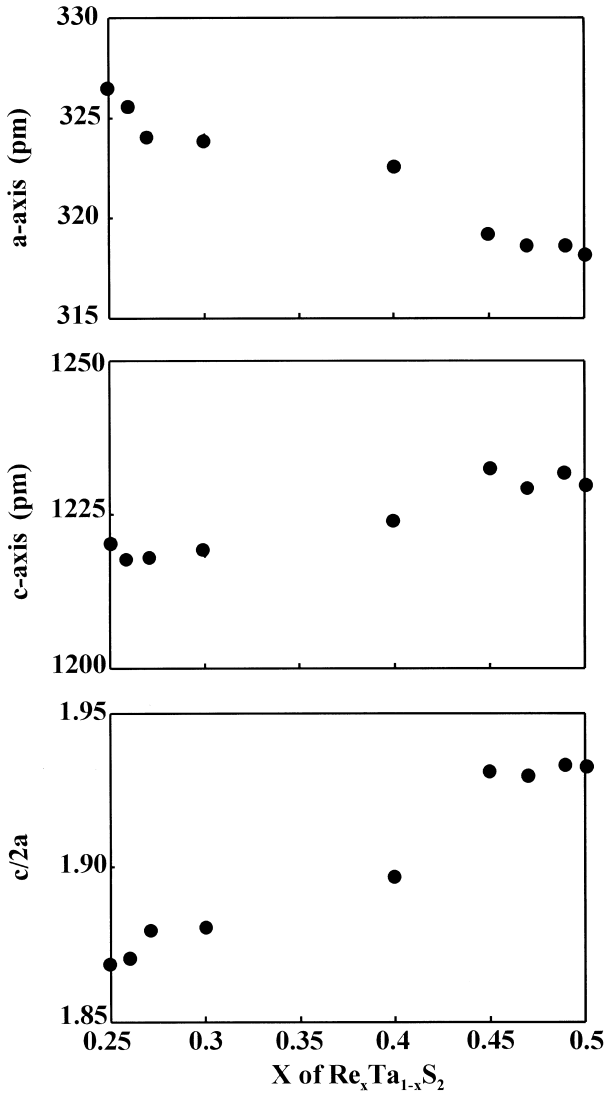

Fig. 4. Lattice parameters of the $Re_xTa_{1-x}S_2$ MLS phase. Top: a-axis, Middle: c-axis, Bottom: axial ratio c/2a. The lattice parameters are calculated on the basis of the 2Hb-polytype hexagonal sublattice.

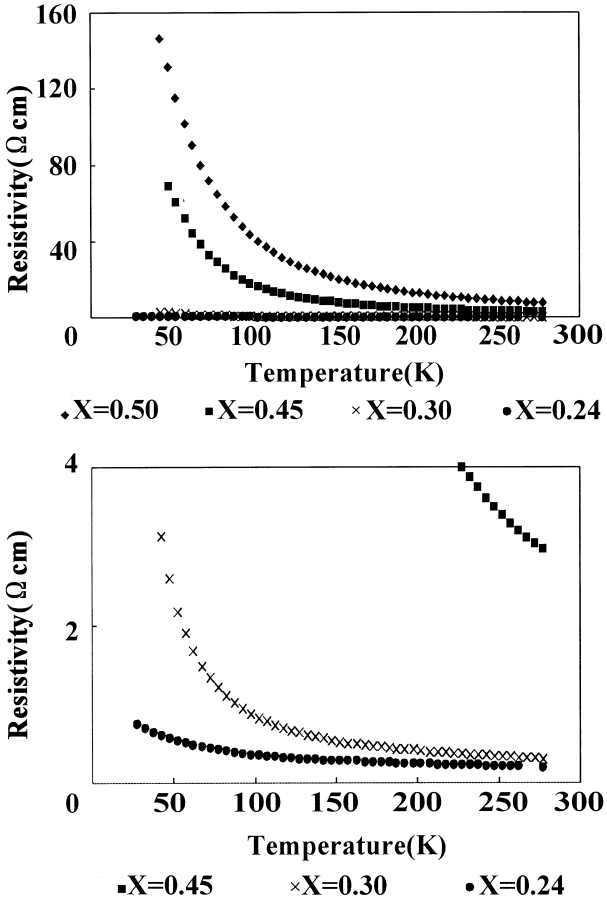

Fig. 5. Electrical resistivity of $Re_xTa_{1-x}S_2$ MLS phase. Top: full range:160 Ω cm, Bottom: full range:4 Ω cm.

However, the ln ρ-1/T plot does not show such a linear relation. The resistivity increases as the x-value increases. This behaviour is similar to that of the $Re_xTa_{1-x}Se_2$ MLS phase.

The temperature dependence of the magnetic susceptibility on the $Re_xTa_{1-x}S_2$ MLS phase is shown in Fig. 6. In this figure the magnetic susceptibility values are not corrected for atom-diamagnetism. The $Re_xTa_{1-x}S_2$ MLS phase shows a weak Pauli- paramagnetism at a high temperature, considering the diamagnetic correction, and shows a weak atom paramagnetism at low temperatures. The magnetic susceptibility values decrease as the x-value increases. In comparison with the results for the resistivity, the Pauli-paramagnetic susceptibility increases as the electrical conductivity increases. These results are consistent with each other when the number of conduction electrons decreases as the x-value increases. This behaviour is similar to that of the $Re_xTa_{1-x}Se_2$ MLS phase.

The small hill around 50 K in the magnetic susceptibility curves is observed. However, there is no anomaly in the corresponding electrical resistivity curves. Therefore the small hill of the magnetic susceptibility curves does not arise from the intrinsic transition but may arise from the extrinsic magnetic susceptibility anomaly.

3.2. OsS_2–TaS_2 system

3.2.1. Phase diagram and structures

The phase diagram from 600 to 1000°C of the OsS_2–TaS_2 system is shown in Fig. 7. The MLS phase spreads over the composition range from $Os_{0.26}Ta_{0.74}S_2$ to $Os_{0.33}Ta_{0.67}S_2$ and the TaS_2 phase, from TaS_2 to $Os_{0.1}Ta_{0.9}S_2$.

Powder X-ray diffraction patterns and simulation patterns of the MLS phase are shown in Fig. 8. The sharp peaks of 00l and hk0 reflections and the broad peaks of hkl reflections are typical features of the MLS's powder X-ray diffraction pattern. The fitting of the

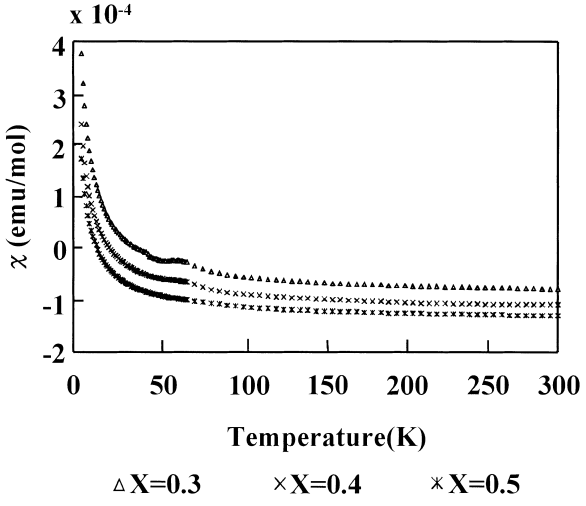

Fig. 6. Magnetic susceptibility of the $Re_xTa_{1-x}S_2$ MLS phase.

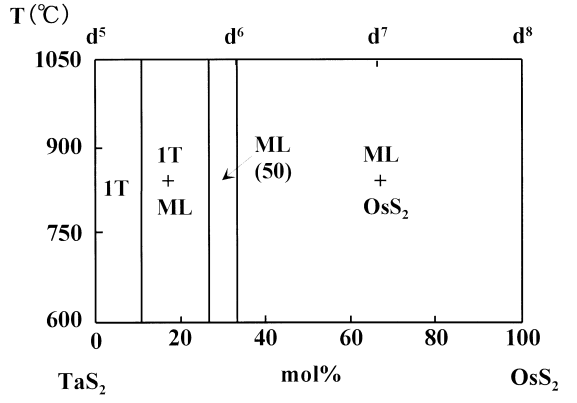

Fig. 7. Phase diagram of the TaS_2–OsS_2 system. ML: MLS phase, (50): 50% 2Hb-layers and 50% 3R-layers, 1 T: CdI_2 type structure.

simulation patterns is satisfactory. All the simulation patterns are calculated on the basis of the random stacking model of 50% 2Hb-layers and 50% 3R-layers. Therefore, the MLS of $Os_xTa_{1-x}S_2$ is constructed by randomly stacking 50% 2Hb-layers and 50% 3R-layers over the homogeneity range.

The homogeneity range of the MLS phase $Os_xTa_{1-x}S_2$ is narrower than that of $Os_xTa_{1-x}Se_2$ because that of the MLS phase $Os_xTa_{1-x}Se_2$ is $0.10 \leqslant x \leqslant 0.33$.[3] The variants of the MLS of $Os_xTa_{1-x}S_2$ are less than those of $Os_xTa_{1-x}Se_2$ because the $Os_xTa_{1-x}Se_2$ MLS and the 2Hb-random stacking structure are only observed. Especially, the layers of the 2Hb–$Os_{0.33}Ta_{0.67}Se_2$ phase stack perfectly at a high temperature. However, the mixing ratio of the 2Hb-layers and 3R-layers is not influenced by temperature. Therefore, the phase relation of the sulfide system may correspond to the low temperature part of the selenide system.

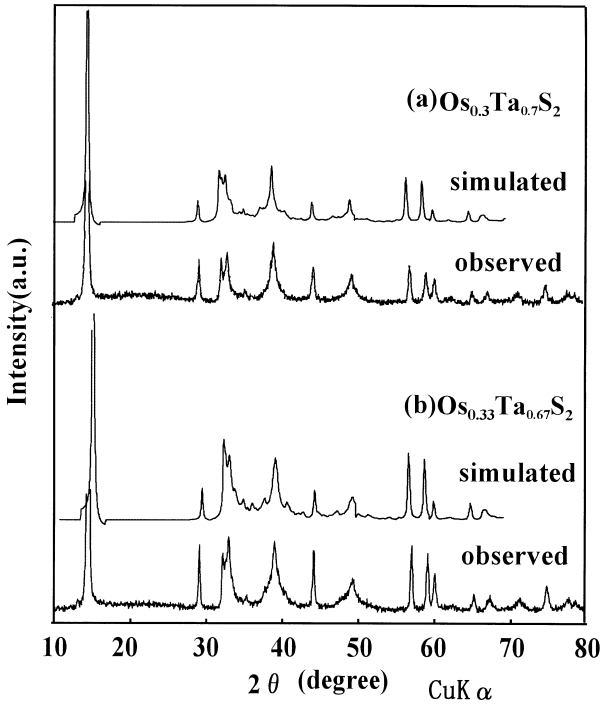

Fig. 8. X-ray powder diffraction patterns of the $Os_xTa_{1-x}S_2$ MLS phase. (a) $x=0.3$, (b) $x=0.33$. Upper patterns are simulated and lower ones are observed.

The homogeneity range of $Os_xTa_{1-x}S_2$ is narrower than that of $Re_xTa_{1-x}S_2$. From the point of the number of valence electrons, $x=0.33$ of $Os_xTa_{1-x}S_2$ corresponds to $x=0.5$ of Re_x $Ta_{1-x}S_2$ but $x=0.26$ of Os_x $Ta_{1-x}S_2$ corresponds to $x=0.39$ of $Re_xTa_{1-x}S_2$, which is larger than the observed value $x=0.25$ of Re_x $Ta_{1-x}S_2$. The homogeneity range of $Os_xTa_{1-x}S_2$ is narrower than that of $Re_xTa_{1-x}S_2$ when taking into account the number of valence electrons.

The lattice parameters of the $Os_xTa_{1-x}S_2$ MLS phase are shown in Fig. 9. The c-parameter represented in this figure is reduced to that of the 2Hb-polytype. The a-parameter decreases, and the c-parameter and the axial ratio c/2a increase as the x-value increases. These features of the $Os_xTa_{1-x}S_2$ MLS phase are similar to those of the $Os_xTa_{1-x}Se_2$ MLS phase, and are common in the sulfide system and selenide system. Moreso, the elongation of the c-axis may be explained by the repulsion of the electrons of the d_{z^2} orbital on a transition-metal atom against the electrons of the p_z-orbital on a sulfur atom.

The features of the lattice parameter on the Os_x $Ta_{1-x}S_2$ MLS phase are similar to those of the Re_x $Ta_{1-x}S_2$ MLS phase except for the chemical composition.

3.2.2. Electrical resistivity and magnetic susceptibility

The temperature dependence of the electrical resistivity of the $Os_xTa_{1-x}S_2$ MLS phase is shown in Fig. 10.

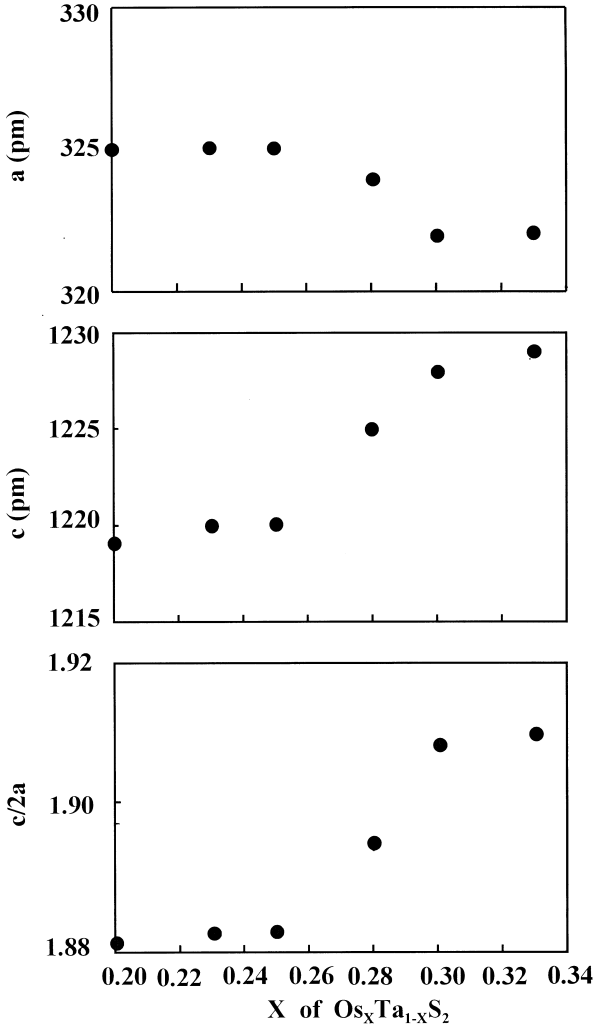

Fig. 9. Lattice parameters of the Os_xTa_{1-x} S_2 MLS phase. Top: a-axis, Middle: c-axis, Bottom: axial ratio c/2a. The lattice parameters are calculated on the basis of the 2Hb-polytype hexagonal lattice.

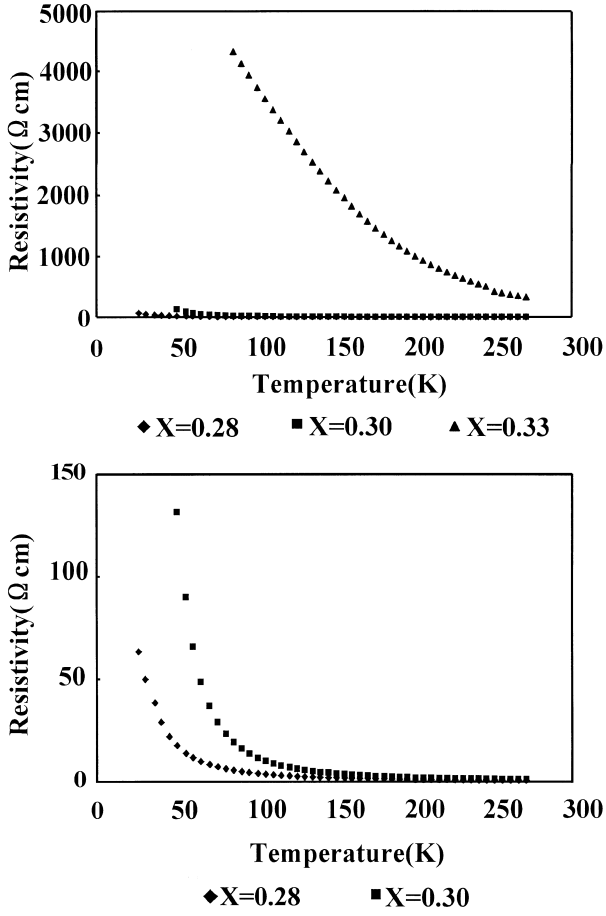

Fig. 10. Electrical resistivity of the $Os_xTa_{1-x}S_2$ MLS phase. Top: full range: 5000 Ω cm, Bottom: a part of (a), full range:150 Ω cm.

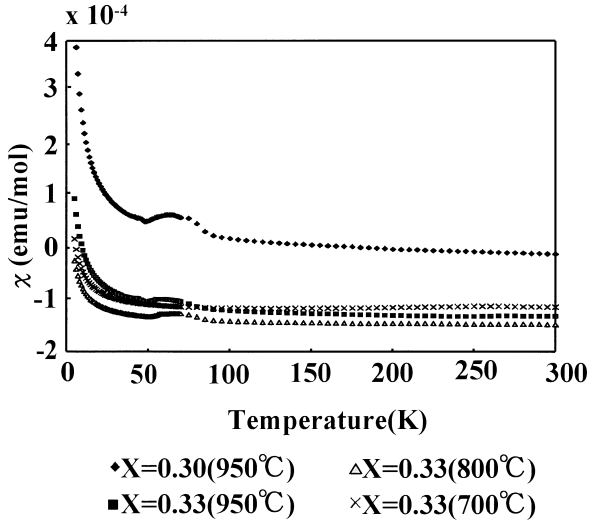

Fig. 11. Magnetic susceptibility of the $Os_xTa_{1-x}S_2$ MLS phase.

The resistivity increases as the temperature decreases. This tendency seems to be that of a semiconductor. However, the ln ρ-1/T plot does not show such a linear relation. The resistivity increases as the x-value increases. These features are similar to those of the Os_x-$Ta_{1-x}Se_2$ MLS phase.

The temperature dependence of the magnetic susceptibility of the $Os_xTa_{1-x}S_2$ MLS phase is shown in Fig. 11. The magnetic susceptibility values are not corrected for atom-diamagnetism. The $Os_xTa_{1-x}S_2$ MLS phase shows a weak Pauli-paramagnetism at a high temperature, considering the diamagnetic correction, and shows a weak atom paramagnetism at a low temperature. The magnetic susceptibility values decrease as the x-value increases. In comparison with the results of the resistivity, the Pauli-paramagnetic susceptibility increases as the electrical conductivity increases. These results are consistent with each other when the number of conduction electrons decreases as the x-value increases. These features are similar to those of the Os_x-$Ta_{1-x}Se_2$ MLS phase. The behaviour of the electrical resistivity and magnetic susceptibility of the Os_x

$Ta_{1-x}S_2$ MLS phase is similar to that of the $Re_xTa_{1-x}S_2$ MLS phase. However, the resistivity and the paramagnetic moment of the $Os_xTa_{1-x}S_2$ MLS phase are larger than those of the $Re_xTa_{1-x}S_2$.

The magnetic susceptibility curves of the samples prepared at various temperatures are similar with each other and the difference of magnetic susceptibility values is small as seen in Fig. 11. Hence the electronic state is changed by the chemical composition difference rather than by the preparation temperature difference.

The small hill around 50 K in the magnetic susceptibility curves is observed. However, there is no anomaly in the corresponding electrical resistivity curves. Therefore the small hill of the magnetic susceptibility curves does not arise from the intrinsic transition but may arise from the extrinsic magnetic susceptibility anomaly.

4. Conclusions

The MLS phases of tantalum rhenium disulfide and tantalum osmium disulfide are prepared.

The homogeneity ranges of the sulfide systems are narrower than those of the selenide systems. The metal ratio of the tantalum poor end of the homogeneity range in the sulfide systems is the same as that in the selenide systems. The perfect stacking 2Hb structures are observed in the selenide systems, however; only random MLS stacking structures are observed in the sulfide systems. The homogeneity ranges of the MLS tantalum rhenium dichalcogenides are wider than those of the MLS tantalum osmium dichalcogenides.

The behaviour of the magnetic susceptibility and the electrical resistivity of the MLS tantalum rhenium disulfide and the tantalum osmium disulfide are similar to those of the MLS tantalum rhenium diselenide and the tantalum osmium diselenide, respectively. The electrical conductivity and the paramagnetic susceptibility of the above systems increase as the tantalum ratio increases. The behaviour of the magnetic susceptibility and the electrical resistivity of the MLS double metal disulfides are explained by the increments of the number of conduction electrons to the increments of the tantalum ratio. Therefore, the electrical conductivity and the Pauli-paramagnetism increase as the tantalum ratio increases.

The MLS phases of the transition metal dichalcogenide systems are the promising candidates for a high-efficiency microwave absorber. The tentative result of the microwave absorption at 2.45 GHz for $Re_xTa_{1-x}S_2$ is shown in Fig. 12. The maximum microwave absorption is observed on the sample $Re_{0.3}Ta_{0.7}S_2$. This value is comparable with that of $Re_{0.3}Nb_{0.7}S_2$ listed in Table 1. More extensive research is necessary in order to develop the practical use of the compounds and to establish the chemistry and physics of the MLS compounds.

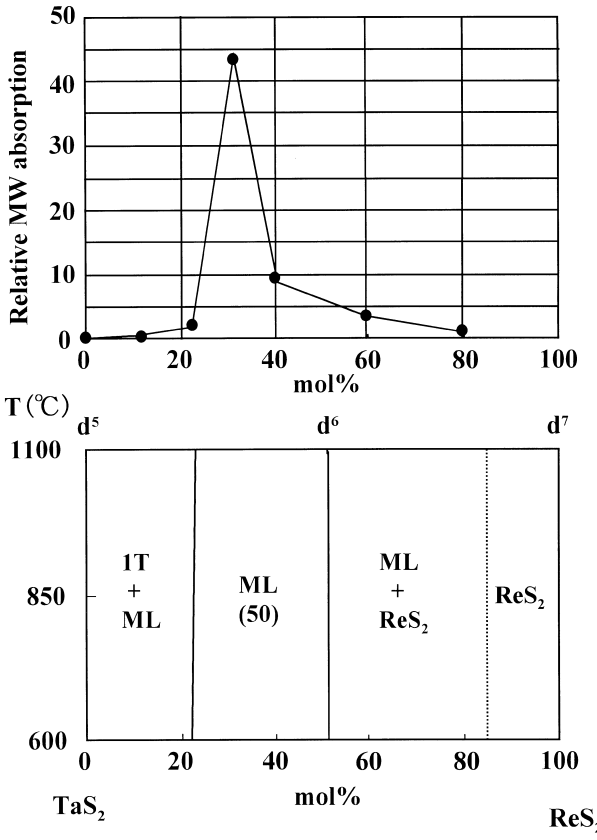

Fig. 12. Microwave absorption of the $Re_xTa_{1-x}S_2$ MLS phase, and the TaS_2–ReS_2 phase diagram.

Table 1
Maximum value of relative microwave absorption for transition-metal dichalcogenides

Compound	Maximum value of relative microwave absorption	Reference
20 mesh Fe-powder	1	1
$Ru_{0.1}Nb_{0.9}S_2$	12	1
$Re_{0.3}Nb_{0.7}S_2$	40	1
$Ru_{0.12}Nb_{0.88}Se_2$	28	1
$Re_{0.2}Nb_{0.8}Se_2$	23	1
$Os_{0.15}Nb_{0.85}Se_2$	37	1
$Os_{0.1}Ta_{0.9}Se_2$	31	1
$Re_{0.3}Ta_{0.7}S_2$	44	Present study

Acknowledgements

This work is supported by a special grant for cooperative research administered by the Japan private school promotion foundation and also by the Kajima foundations research grant.

The authors would like to thank Mr Matthew Main for reading the manuscript and offering advice concerning English usage.

References

1. Hayashi, K., Serikawa, D., Chijimatsu, Y., Shimakawa, M., Kume, S., Manabe, K. and Takahashi, T., Microwave absorption of MLS transition-metal dichalcogenides. *J. Alloys Comp*., 1997, **262**(263), 325–330.
2. Hulliger, F., *Structural Chemistry of Layer-Type Phases*. Reidel, Holland, 1976, pp. 219–242.
3. Hayashi, K., Ikeuchi, T., Takeuchi, H. and Shimakawa, M., Mixed layers in $M_xTa_{1-x}Se_2$ (M = Re,Os; $0 < x$). *J. Alloys Comp*., 1995, **219**, 161–167.
4. Furusho, M., Patent, Japan 5-182517(1995.07.23), 4-18490(1994.01.07).
5. Maruyama, Y., personal communication, Okayama University, 1989.